Smart Structures and Systems, *Vol. 28, No. 5 (2021) 617-629*
https://doi.org/10.12989/sss.2021.28.5.617

A new hybrid model for MR elastomer device and parameter identification based on improved FOA

Yang Yu*[1,2], Amir M. Yousefi [2a], Kefu Yi [3a], Jianchun Li [1a], Weiqiang Wang**[4a] and Xinxiu Zhou [5a]

[1] *School of Civil and Environmental Engineering, University of Technology Sydney, Ultimo, NSW 2007, Australia*
[2] *Centre for Infrastructure Engineering, Western Sydney University, Penrith, NSW 2751, Australia*
[3] *School of Automotive and Mechanical Engineering, Changsha University of Science and Technology, Changsha 410114, China*
[4] *College of Water Conservancy and Hydropower Engineering, Hohai University, Nanjing, Jiangsu 210098, China*
[5] *Research Institute for Frontier Science, Beihang University, Beijing 100191, China*

(*Received February 19, 2021, Revised July 2, 2021, Accepted July 15, 2021*)

Abstract. A new hysteresis model based on curve fitting method is presented in this work to portray the greatly nonlinear and hysteretic relationships between shear force and displacement responses of the magnetorheological (MR) elastomer base isolator. Compared with classical hysteresis models such as Bouc-Wen or LuGre friction model, the proposed model combines the hyperbolic sine function and Gaussian function to model the hysteretic loops of the device responses, contributing to a great decline of model parameters. Then, an improved fruit fly optimization algorithm (FOA) is proposed to optimize the model parameters, in which a self-adaptive step is employed rather than the fixed step to balance the global and local optimum search abilities of algorithm. Finally, the experimental results of the device under both harmonic and random excitations are used to verify the performance of the proposed hybrid model and parameter identification algorithm with the satisfactory results.

Keywords: base isolator; fruit fly optimization algorithm (FOA); hybrid model; magnetorheological (MR) elastomer

1. Introduction

Magnetorheological (MR) elastomer is a type of intelligent material, which is composed of high-permeability particles blended in the nonmagnetic elastomer matrix (Zhang and Li 2009, Wen *et al*. 2017, Bastola and Li 2018). Under external magnetic field, the stiffness and damping properties of the MR elastomer can be quickly, continuously and reversibly tuned (Aziz *et al*. 2018, Nguyen *et al*. 2018). Due to this inherent characteristic, MR elastomer-based devices have been recently developed as the promising candidates for vibration mitigation and isolation of civil infrastructure like buildings and bridges subjected to hazard external excitations such as strong winds, earthquakes and destructive shocks (Sun *et al*. 2017, Xin *et al*. 2017, Ying *et al*. 2017, Hwang *et al*. 2020). Nevertheless, the main challenge that will affect their actual practice is dynamic modeling of complicated input and output relationships of unique features of device responses. Respecting adaptive control of building structures, it is of great importance that a robust device model should be established before any control method is used in implementation (Zhou *et al*. 2020).

To date, several hysteresis models have been reported in literatures based on a series of techniques, which can be used to characterize the nonlinear behaviours of MR elastomer devices. Models acquired by the conclusive method contain Bouc-Wen model (Yang *et al*. 2013, Behrooz *et al*. 2014, Zhu and Rui 2014), Dahl model (Aguirre *et al*. 2012, Piatkowski 2014), LuGre friction model (Jiménez and Álvarez-Icaza 2005, Piatkowski 2014) and strain stiffening model (Li and Li 2019). These models employed various differential equations to portray the nonlinearly hysteretic loops with medium or high complexities. However, in the viewpoint of real-time control, the nonlinear differential equations in the models will influence the stability of the designed controller when the MR elastomer devices are utilized in the seismic mitigation of building structures. Besides, soft computing methods, such as artificial neural networks (ANN), support vector machine (SVM) and adaptive neuro fuzzy inference system (ANFIS) were employed to set up nonparametric models for MR elastomer devices (Fu *et al*. 2020, Leng *et al*. 2020). In spite of promising application prospect, these methods need to adjust the network structure so as to obtain an accurate and robust model. Furthermore, nonparametric models are not able to directly depict the mechanical relationships between hysteretic responses and model parameters. However, in the practical application, a model with explicit physical explanations to hysteretic loops is satisfying.

On the other hand, evolutionary optimization techniques such as genetic algorithm and particle swarm optimization have been developed in the applications of modeling and parameter identification of MR elastomer devices, which are mainly inspired by biological behaviours of species. More recently, a new swarm evolutionary algorithm called

*Corresponding author, Ph.D.,
E-mail: yang.yu@uts.edu.au; ww674@uowmail.edu.au
**Co-corresponding author, Ph.D.

ISSN: 1738-1584 (Print), 1738-1991 (Online)

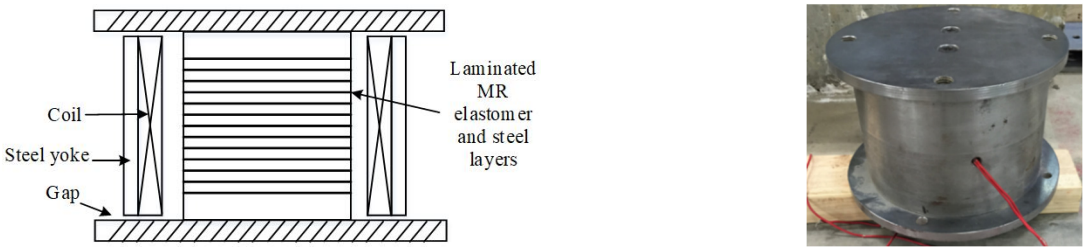

(a) Schematic figure (b) Real objective

Fig. 1 Adaptive MR elastomer base isolator

fruit fly optimization algorithm (FOA) was proposed by Pan, which was based on the food search behaviour of fruit fly swarm (Pan 2013). The main idea of FOA is that the fruit fly has more superior osphresis sensing and vision perception than other animals. Because it is easy to understand and to be implemented as the program codes, FOA has been utilized in many application fields. Niu *et al*. employed FOA to estimate the coal gasification (Niu *et al*. 2015). Lin adopted FOA to optimize the weights of neural networks to analyze the service satisfaction in web auction logistics service (Lin 2013). Li *et al*. combined FOA with least square support vector machine to establish a regression model for electric load prediction (Li *et al*. 2018). FOA was also found to successfully solve the path planning problem for the unmanned aerial vehicle (UAV) (Zhang *et al*. 2018). Although FOA has the advantages of fewer algorithm parameters and rapid convergence, it always undergoes the premature or local optimum when dealing with multi-variable optimization problems. In consideration of this drawback of FOA, this work presents an improved FOA, which adopts a self-adaptive update strategy to real-timely update the step length for balancing the global and local optimization capacities in different iteration stages.

This study aims to characterize highly nonlinear behavior of MR elastomer base isolator, which exhibits the hysteresis in force-displacement/velocity responses, via phenomenological modeling. As all we know, to fully apply smart isolator in structural vibration isolation, the proposed model should be with comprehensive ability in portraying hysteretic responses of the device under a variety of external excitations. Hence, dynamic tests of MR elastomer base isolator are first conducted with different loading frequencies and amplitudes as well as different levels of current input. Then, based on test results, a novel hybrid model based on curve fitting approach is proposed for characterizing hysteretic force-displacement/velocity responses. In this model, a hyperbolic sine function and a Gaussian function are used to express the mean values and thickness of hysteresis loops, respectively. Mixture of both functions is able to effectively describe the nonlinear and hysteretic relationships between shear force and displacement responses of the device. Model parameter estimation is transformed as solving a minimization optimization problem, in which a fitness function is built based on the root mean square (RMS) errors between experimental and estimated data. Using the proposed self-adaptive step-based FOA, the model parameters could be optimized synchronously based on experimental input and output responses from different loading conditions. The performances of the proposed model and algorithm are verified through comparisons with other conventional hysteresis models and optimization algorithms. Finally, a generalized model based on field-dependent parameters is contributed to make it more adaptive for control application.

2. Experimental testing of adaptive MR elastomer isolator

The newly designed MR elastomer isolator adopted a laminated structure in traditional rubber bearings, which contains 25 layers of MR elastomer sheets and 24 layers of steel sheets together with cylindrical steel yoke and electromagnetic coil as shown in Fig. 1. To characterise the nonlinear mechanism of the device, several tests were conducted using a shake table, which is able to provide the horizontal excitations, shown in Fig. 2. In the experimental setup, a load cell was installed to measure the transversal force loaded to the device, which was installed on the shake table and moves with the motion of table. A DC power supply and a slider were utilized to provide and control the supply current to the magnetic coil. The specific information on experimental setup can be referred in Li and Li (2019), and the information of steel material used can be found in Yousefi *et al*. (2020).

As the main seismic frequency bands are always in the range of [0 10 Hz], the experiments were proposed with the

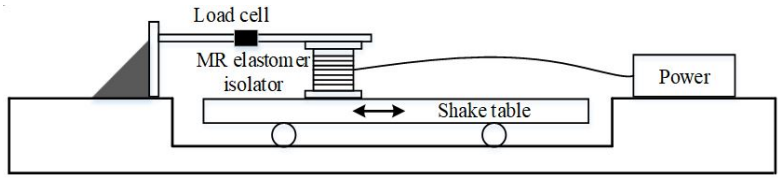

Fig. 2 Sketch of experimental setup

input frequency below 10 Hz. Two types of excitation waveforms were selected in this work: sinusoidal and random wave loadings. For the sinusoidal inputs, the excitation amplitudes were 2, 4 and 8 mm, and the fixed loading frequencies were 1, 2 and 4 Hz, respectively. For the random inputs, the maximum excitation amplitude was 4 mm and excitation frequencies were set between 1 Hz and 10 Hz. During the testing, the MR elastomer base isolator was applied with different current levels from 0 A to 3 A to evaluate its field-dependent properties. The data was collected with a 256 Hz sampling frequency and a 5 s sampling period. The displacement and shear force responses of the device could be directly measured from displacement sensor in the shake table and load cell while the velocity responses were obtained from differential calculation of time-displacement responses.

Fig. 3 shows the field-dependence behaviour of the MR elastomer isolator, when it is excited by sinusoidal loading with 2 Hz frequency and 4mm amplitude, in which Fig. 3(a) shows the force-displacement responses and Fig. 3(b) portrays the force-velocity hysteretic loops. It is noticeable from both figures that the force-displacement responses go on to clockwise path while the force-velocity loops follow counter clockwise direction. Besides, it can be found from the loop shape that the isolator operates more like the variable stiffness device, which can be supported by almost linear relationship between force and displacement responses. Moreover, when the device is at the location of maximum displacement (where the device velocity is 0), the shear force is in close proximity to the peak value, which indicates that the main contribution of the force comes from the stiffness. On the contrary, the displacement of the isolator is 0 (where maximum velocity happens), the value of the shear force is minimal. Furthermore, the peak force and energy dissipation capacity of the device, which is represented by the enclosed area of force-displacement loop, are enhanced with the increase of the applied current. Accordingly, to make full use of this innovative MR elastomer device, a robust and accurate model that is capable of describing these field-dependent properties is highly required. The detailed procedure for modeling MR elastomer isolator will be presented in the next section.

3. Hybrid hysteresis model for MR elastomer isolator

3.1 Model design

The proposed model is designed based on curve fitting method, in which the hyperbolic sine function is adopted to portray the mean hysteresis of force-displacement response and the Gaussian function is used to represent the thickness of the hysteretic response. Therefore, the captured responses can be regarded as the combination of two sub responses, which can be expressed by average and thickness curves of the hysteretic responses.

Fig. 4(a) gives the one example of typical force-displacement response of MR elastomer base isolator when the device is driven with 8 mm loading amplitude, 4 Hz excitation frequency and 1 A magnetization current. This response curve can be divided into two parts: the upper part P_1 when the velocity of the device is positive and the lower part P_2 when the velocity is negative. First, the average value of response cycle is able to be calculated through taking the mean value of each vertical component in the hysteretic loops, shown as Eq. (1)

$$\bar{X}_i = \frac{1}{N}\sum_{i=1}^{N}(P_{1,i} + P_{2,i}) \tag{1}$$

where i denotes the sample index of measured device displacement; $P_{1,i}$ and $P_{2,i}$ denote the shear forces generated by the MR elastomer base isolator corresponding to the displacement polarity, respectively. Then, a hyperbolic sine function based curve is utilised to depict this mean value curve, which is made up of three parameters, shown as

$$G(x) = \alpha \cdot \frac{e^{2\beta x} - 1}{2e^{\beta x}} + F_0 \tag{2}$$

where F_0 denote the initial force of the device, which can be obtained by averaging the maximum and minimum force values in one cycle; α and β are two parameters to be identified. The example of comparison between results from the experimental measurements and predictions from hyperbolic sine function is shown in Fig. 4(b).

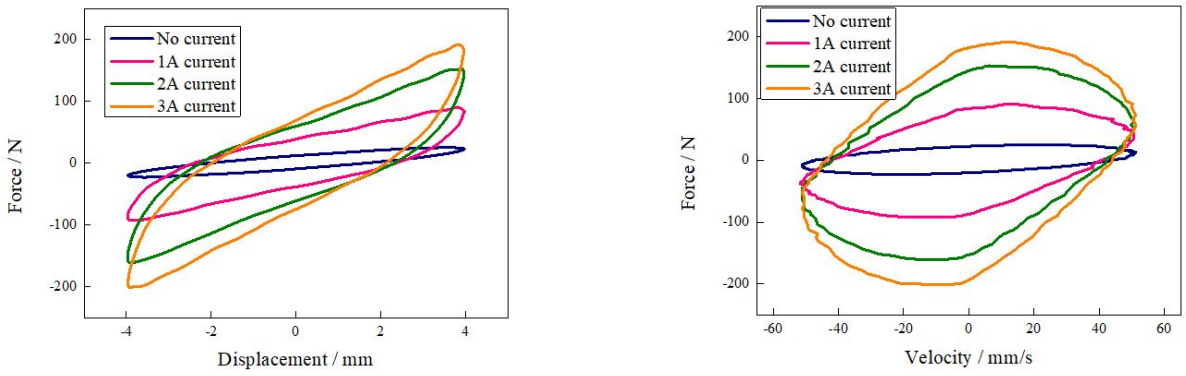

(a) Force-displacement response (b) Force-velocity response

Fig. 3 Testing results of MR elastomer isolator under sinusoidal loading with different applied currents (2 Hz-4 mm)

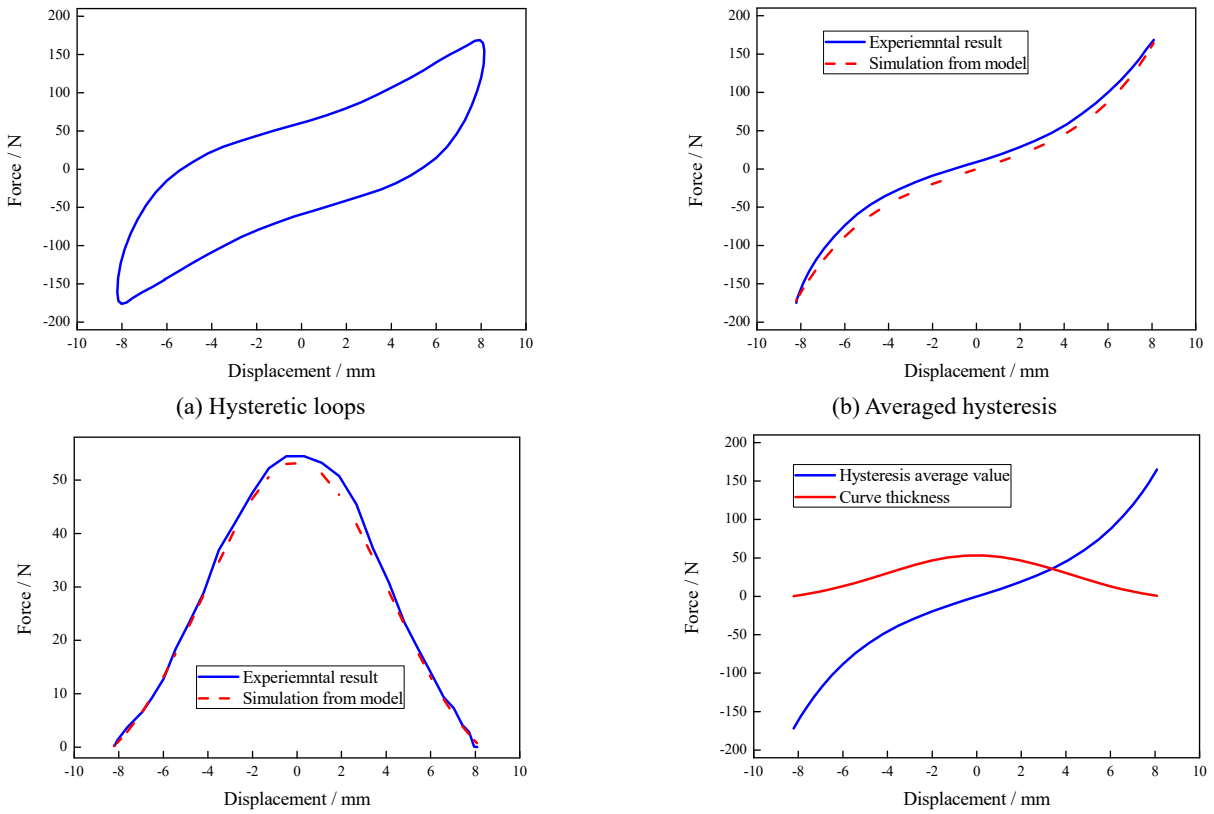

(a) Hysteretic loops (b) Averaged hysteresis

(c) Thickness of hysteresis (d) Average and thickness curves of hysteresis

Fig. 4 Modeling of MR elastomer isolator based on curve fitting

Furthermore, the hysteresis thickness is able to be obtained by calculating the average difference between responses from upper as well as lower parts and average hysteresis responses, shown in Fig. 4(c). The mathematical expression to calculate hysteresis thickness is given as

$$T_i = \frac{1}{N}\sum_{i=1}^{N}\left(\left|P_{1,i} - \bar{X}_i\right| + \left|P_{2,i} - \bar{X}_i\right|\right) \tag{3}$$

The response curve according to above equation can be precisely described using the Gaussian function with the following expression

$$H(x) = \gamma e^{-\frac{x^2}{2\sigma^2}} \tag{4}$$

where γ and σ represent the vertical scaling parameter and width of the hysteresis, respectively. Finally, the whole hysteretic response can be calculated via the combination of two response components, shown in Fig. 4(d). Through subtracting and adding two elements according to the device velocity, lower and upper part responses will be constructed, respectively. Thus, the mathematical expression of the proposed hybrid model can be concluded as follows

$$F(x) = \begin{cases} F_1(x):\ G(x) + H(x),\ \dot{x} \geq 0 \\ F_1(x):\ G(x) - H(x),\ \dot{x} < 0 \end{cases} \quad \text{or} \tag{5}$$

$$F(x) = \begin{cases} F_1(x):\ \alpha \cdot \dfrac{e^{2\beta x} - 1}{2e^{\beta x}} + \gamma e^{-\frac{x^2}{2\sigma^2}} + F_0,\ \dot{x} \geq 0 \\ F_1(x):\ \alpha \cdot \dfrac{e^{2\beta x} - 1}{2e^{\beta x}} - \gamma e^{-\frac{x^2}{2\sigma^2}} + F_0,\ \dot{x} < 0 \end{cases} \tag{5}$$

where x and $\dot{x}$ denote the displacement and velocity of the device, respectively.

3.2 Problem statement

In comparison with other classical models of MR elastomer devices, the newly proposed hybrid model doesn't contain any differential equation and has fewer parameters to be determined. However, due to high nonlinearity in both hyperbolic sine and Gaussian functions, the model parameters are not easy to be accurately calculated using direct searching algorithms. As a consequence, nonlinear model parameter identification should be converted into solving an optimization problem. The critical issue is to design an appropriate objective function (fitness), which is closely related to the final identification result. In this work, the root mean square (RMS) error is employed to construct the objective function for optimization problem, shown as

$$O(X) = \sqrt{\frac{1}{N}\sum_{i=1}^{N}[F_i^m - F_i(X)]^2} \tag{6}$$

where $X = [\alpha, \beta, \gamma, \sigma^2]$ is the parameter vector to be identified; F_i^m and F_i denote the measured shear force and calculated result from the hybrid model at ith time, respectively. N denotes the total number of measurements used for model identification. If the value of the objective function is close to zero, the corresponding result X can be considered as the best solution. With the constraint conditions, the optimization problem can be depicted as

$$\begin{aligned} &\underset{X}{Min} \;\; Obj = O(X) \\ &s.t. \;\; \alpha > 0, \beta > 0, \gamma > 0 \end{aligned} \tag{7}$$

4. Improved fruit fly optimization algorithm for model identification

4.1 Standard FOA

FOA is a newly proposed swarm-based evolutionary optimization algorithm, which was designed via simulating the feeding behaviour of fruit flies. Due to their superiorities in perception and sensing, the fruit flies are able to rapidly detect various scents using the osphresis organ and rapidly fly with the swarm using vision organ (Pan 2013). The procedure of the fruit fly searching for food is briefly illustrated in Fig. 5, and FOA can be concluded by the following steps:

Step 1. Set the randomly initial position of fly swarm: *x_axis* and *y_axis*;

Step 2. Random orientation and distance are given to each fly for searching food, expressed in Eqs. (8) and (9)

$$x_i = x\_axis + l \cdot rand \tag{8}$$

$$y_i = y\_axis + l \cdot rand \tag{9}$$

where l denotes the step length and *rand* denotes the random number between 0 and 1.

Step 3. Because of unknown food source, the distance D_i between fly's position and original point should be first calculated. Then, its reciprocal R_i is used as smell concentration coefficient

$$D_i = \sqrt{x_i^2 + y_i^2} \tag{10}$$

$$R_i = 1/D_i \tag{11}$$

Step 4. Take the coefficient into the fitness function to calculate the smell concentration value S_i of ith fly at the current position

$$S_i = Fitness(R_i) \tag{12}$$

Step 5. Find out the fruit fly with the best S_i (maximum value) in the whole swarm

$$[best\_S, best\_index] = Max(S_i) \tag{13}$$

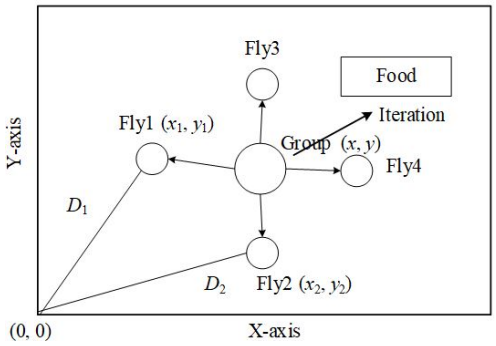

Fig. 5 Basic procedure of FOA

Step 6. Record the optimal S_i together with coordinates of corresponding fruit fly. Then other fruit flies in the swarm fly to this optimal position using vision organ

$$S\_best = best\_S \tag{14}$$

$$x\_axis = x_{best\_index} \tag{15}$$

$$y\_axis = y_{best\_index} \tag{16}$$

Step 7. Repeat the operations from Step 2 to Step 5, and compare current S_i with optimal S_i. If the current value is superior to the optimal value, go to Step 6; or else, go to Step 7 directly.

4.2 Self-adaptive step-based FOA

In the standard FOA, the step length l is generally set as a constant, which means that the individual fly will randomly seek the food source near the swarm by osphresis according to this fixed value. Obviously, when the swarm population is determined, the larger step will result in the larger search space. In this case, the algorithm has the stronger global search ability but weaker local search ability, which makes the algorithm unfavourable in the later stage of iteration. On the contrary, if the value of the step length is too small, the algorithm will have the stronger local search ability, which may lead to limited search space and make the fly fall into the local optimal position. Accordingly, the selection of step length will directly affect the algorithm implementation efficiency. In this paper, for this key issue, an iteratively decreasing step is introduced to substitute for the fixed step in FOA, which can be expressed as

$$l = l_0 \cdot e^{[-10 \cdot (\frac{G}{G_{max}}} \tag{17}$$

where l_0 denotes the initial step length; G and G_{max} denote the current and maximum iteration number, respectively. It is clearly seen that in the initial stage of iteration, the algorithm has strong global search ability so that the fly can move to the approximate position of food source very quickly. With the increase of iteration, the local search ability will be enhanced, guaranteeing that algorithm will not trap into local optimum at the later stage. Therefore, the proposed self-adaptive step-based FOA can effectively realize the balance between global and local search abilities.

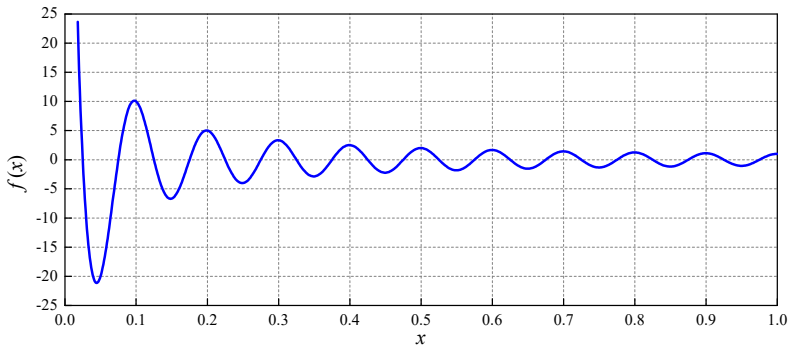

Fig. 6 Curve of cosine gradient function

4.3 Algorithm performance test

In this section, a cosine gradient function is employed to illustrate the superiority of self-adaptive step in FOA, which has one global minimal value and several local minimal values. The expression and curve of sine gradient function are given in Eq. (18) and Fig. 6.

$$f(x) = \frac{cos(20\pi x)}{x}, \quad x \in [0,1] \tag{18}$$

Furthermore, standard FOAs with fixed step 2 and 20 are used for performance comparison. For the self-adaptive step FOA, the initial step value is set as 20, and population number and maximum iteration are set as 10 and 50 for all three types of FOAs. After maximum iteration, the flight paths of fruit flies and variation curve of smell using three FOAs are shown in Figs. 7, 8 and 9, respectively. Fig. 7 gives the optimization results using self-adaptive step FOA. It is noticeable from the figure that the algorithm has larger search range as well as stronger global search ability, which

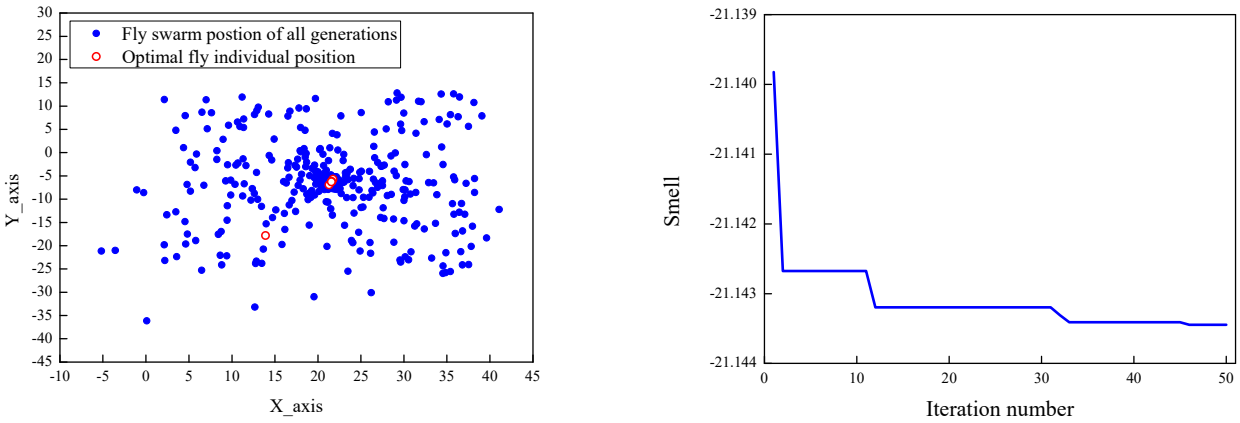

(a) Foraging path of individual fly (b) Smell convergence

Fig. 7 Optimization procedure using self-adaptive step-based FOA

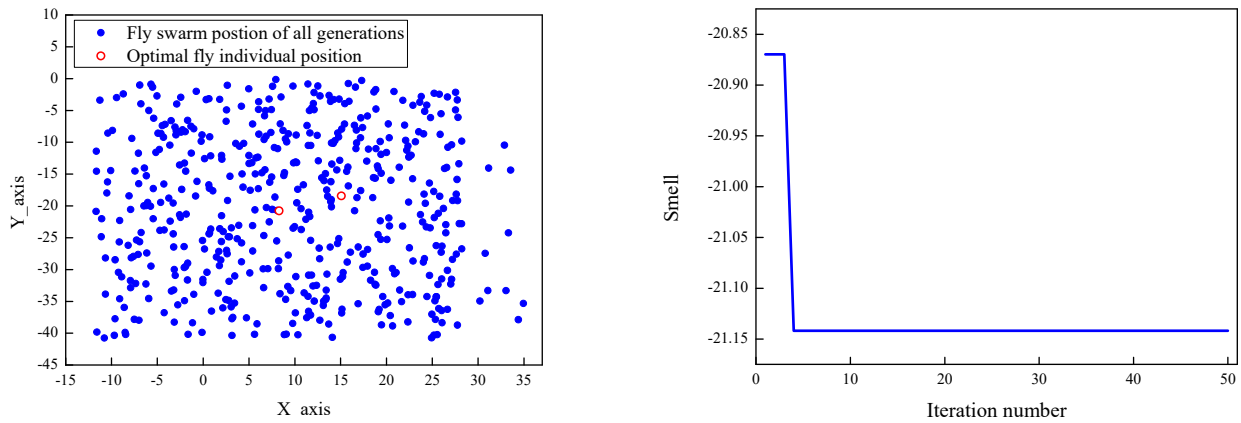

(a) Foraging path of individual fly (b) Smell convergence

Fig. 8 Optimization procedure using FOA with fixed step 20

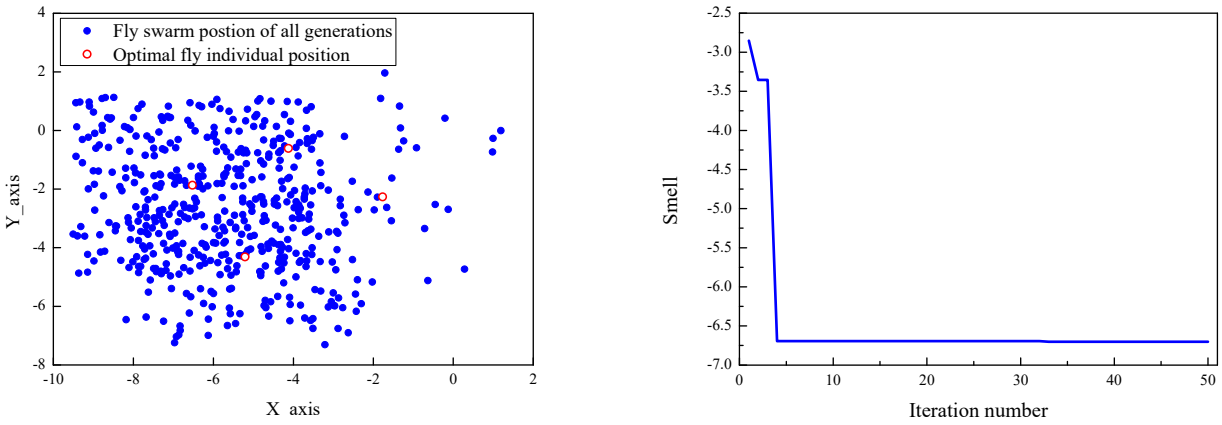

(a) Foraging path of individual fly (b) Smell convergence

Fig. 9 Optimization procedure using FOA with fixed step 2

makes fitness value arrive at -21.139 after the first iteration. Then, with the adding iteration, the result is gradually close to the optimal solution. In the later stage, the algorithm has strong local search ability to slightly adjust the optimal value, and obtain the global optimum -21.143 at 46th iteration. Besides, the flight path reflects the evolutionary process of fly swarm, which is from sparseness to denseness.

Figs. 8 and 9 give the optimization results using FOA with fixed steps 20 and 2 respectively. When the step length equals to 20, the algorithm has the strong global search ability and the fitness value will arrive at its optimum -21.142 at 4th iteration. Then, the fitness value is unchanged until the algorithm terminates. It is clearly seen that individual fly shows the uniform distribution in the area of ([-15, 30], [-40, 0]), which also verifies that the fixed larger step can cause the weak local search ability of FOA in the later stage of algorithm iteration. When the value of step length is 2, the fitness value will reach its optimum -6.694 at 4th iteration. It is obviously illustrated that the small fixed step will cause weak global search ability, and makes the algorithm premature. It can also be reflected from Fig. 9(a) that the fruit fly uniformly moves in a relatively small search space ([-10, 0], [-8 2]), and cannot jump out of the local optimal solution. From the above analysis, the proposed self-adaptive step-based FOA is able to maintain the variable-scale searching in the iteration process, balance both global and local search abilities, and finally obtain the better identification result.

5. Result and discussion

In this work, self-adaptive step-based FOA is compiled using MATLAB v.2015a. The parameters of proposed hybrid model are offline estimated based on the experimental results from harmonic excitations. Fig. 10 gives one case of optimal flight path of fruit fly to search the model parameter α when the device was driven with a 2 Hz frequency, 4 mm amplitude excitation and 1 A supply current. It is clearly seen that the fly swarm arrives at the approximately optimal position very quickly due to the strong global search ability. Then, near the optimal position, the fruit fly carries out the local search for optimal solution using gradually declining step length and finally finds the global optimum after several trials. To verify the superiority of the proposed FOA method in model identification of MR elastomer base isolator, other conventional swarm-based optimization algorithms such as genetic algorithm (GA), particle swarm optimization (PSO) and artificial fish swarm algorithm (AFSA) are utilized for performance comparison. To fairly compare the algorithm performance, population and maximal iteration numbers of all the algorithms are set as 50 and 500, respectively. Other parameter settings in different algorithms can be referred to (Neshat *et al*. 2014, Tairidis *et al*. 2016, Trivedi *et al*. 2016). Fig. 11 shows the convergence variations with the adding iteration of four algorithms when they are used to identify the proposed model based on the same experimental data (2 Hz-4 mm-1 A). The results show that the AFSA presents the fastest convergence among all methods, but it has the largest fitness value (RMS), which means that it causes the premature convergence. Although the proposed improved FOA arrives at the global optimal value much more slowly than GA and PSO, it has the highest identification accuracy. The main reason for this result is that the improved FOA adopts self-adaptive step length update mechanism. At the later stage of algorithm evolution, a smaller value of step

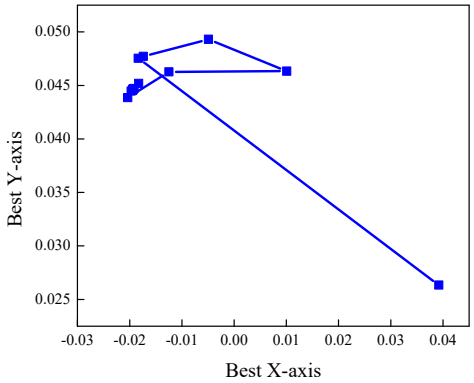

Fig. 10 Best flight path of parameter *α*

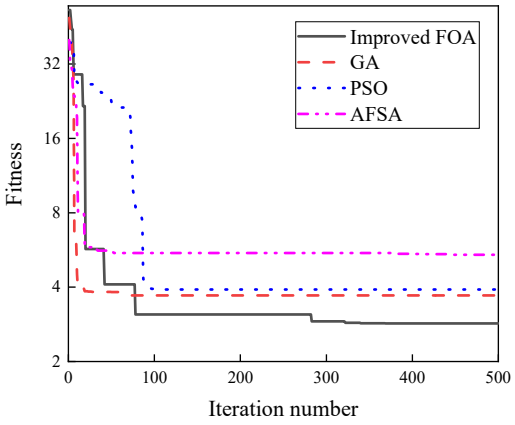

Fig. 11 Convergence comparison among four algorithms

length is assigned to the fruit fly, which enhances the exploitation ability of algorithm. At this stage, local adjustment is conducted to fine-tune the solution to improve the accuracy. Therefore, the improved FOA is an ideal candidate for modeling and parameter identification of MR elastomer base isolator. Using this advanced algorithm, the parameter values of proposed hybrid model corresponding to all the loading conditions are identified and the results are presented in Tables 1-4.

To validate the capacity of the proposed hybrid model to characterize the unique behaviours of this novel adaptive device, several sets of comparisons are conducted between experimental measurements and models predictions. Fig. 12 studies the influence of excitation frequency on the system output responses. It is obviously seen that the displacement-force responses are independent of loading frequency although an increasing excitation frequency will produce the ascending nonlinear velocity-force responses. Besides, it is clear that the results predicted from the proposed model perfectly accord with the testing data, which directly proves that the model is able to well portray this frequency-independent feature.

Figs. 13(a) and (b) investigate the effects of loading amplitude and supply current on the output shear force, respectively. It can be noticed from Fig. 13(a) that the excitation amplitude plays an inverse role on the effective stiffness, denoted by the slope of the response loops, which means that the adding amplitude results in a slightly decreasing effective stiffness. This property is also called

Table 1 Identification results of parameter α under different loading conditions

Loading condition		Current level			
Amplitude	Frequency	0 A	1 A	2 A	3 A
2 mm	1 Hz	32.02	43.75	41.77	56.87
	2 Hz	37.66	42.49	54.92	68.33
	4 Hz	6.51	54.57	59.39	50.99
4 mm	1 Hz	40.74	43.81	44.21	53.76
	2 Hz	48.34	20.55	60.76	79.26
	4 Hz	44.69	64.26	66.78	66.35
8 mm	1 Hz	26.06	52.82	64.31	44.67
	2 Hz	50.61	36.13	33.47	72.97
	4 Hz	36.82	41.14	56.97	69.04

Table 2 Identification results of parameter β under different loading conditions

Loading condition		Current level			
Amplitude	Frequency	0 A	1 A	2 A	3 A
2 mm	1 Hz	0.75	0.67	0.86	0.82
	2 Hz	0.47	0.67	0.72	0.72
	4 Hz	0.85	0.58	0.69	0.88
4 mm	1 Hz	0.38	0.43	0.51	0.52
	2 Hz	0.39	0.38	0.42	0.42
	4 Hz	0.31	0.44	0.41	0.46
8 mm	1 Hz	0.25	0.28	0.27	0.34
	2 Hz	0.29	0.27	0.35	0.28
	4 Hz	0.25	0.29	0.28	0.28

Table 3 Identification results of parameter γ under different loading conditions

Loading condition		Current level			
Amplitude	Frequency	0 A	1 A	2 A	3 A
2 mm	1 Hz	1.54	15.41	24.73	24.56
	2 Hz	2.26	16.87	27.77	28.99
	4 Hz	2.88	19.78	31.19	31.97
4 mm	1 Hz	3.07	21.92	32.51	35.78
	2 Hz	4.47	24.87	37.04	38.08
	4 Hz	6.41	28.39	42.62	44.49
8 mm	1 Hz	5.99	30.87	45.67	48.01
	2 Hz	9.09	36.55	52.51	55.77
	4 Hz	12.75	44.69	61.99	66.36

Table 4 Identification results of parameter σ^2 under different loading conditions

Loading condition		Current level			
Amplitude	Frequency	0 A	1 A	2 A	3 A
2 mm	1 Hz	2.83	1.87	1.73	1.63
	2 Hz	3.13	2.03	1.89	1.88
	4 Hz	4.23	2.42	2.13	2.07
4 mm	1 Hz	8.57	6.85	6.49	6.11
	2 Hz	10.18	7.61	7.28	6.98
	4 Hz	10.92	9.96	8.53	8.99
8 mm	1 Hz	23.25	25.64	24.89	23.98
	2 Hz	22.89	28.13	28.23	27.82
	4 Hz	28.59	34.01	34.02	33.25

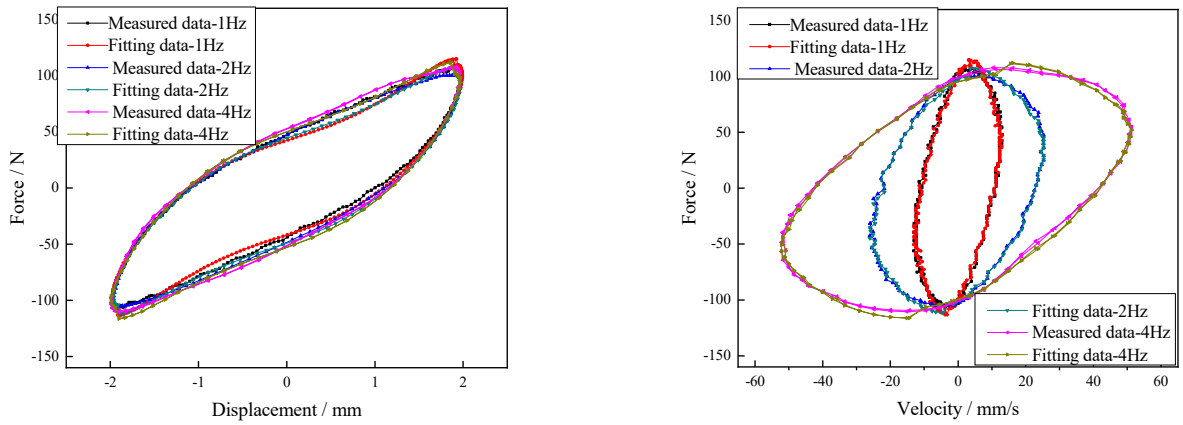

(a) Force-displacement response (b) Force-velocity response

Fig. 12 Comparison between experimental data and fitting data with different excitation frequencies

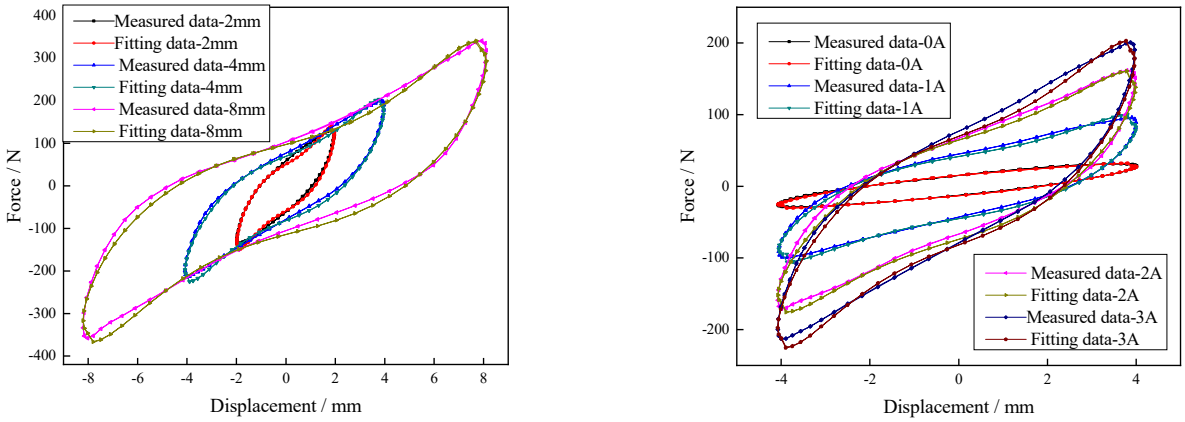

(a) Responses with different amplitudes (b) Responses with different currents

Fig. 13 Force-displacement responses comparison between experimental data and fitting data

Mullins effect (Mullins and Tobin 1957). Different from loading amplitude, the increasing supply current will induce an adding effective stiffness, shown in Fig. 13(b). When there is no current applied to the device, the response turns out to be almost liner force-displacement relationship. However, when the supply current gradually increases, the nonlinear force-displacement loops become more obvious. This phenomenon is called strain stiffening (Besdo and Ihlemann 2003). The good match between the predictions and experimental data demonstrates that the proposed model is also capable of effectively characterizing these features of the device.

To illustrate the superiority of the proposed hybrid model, a comparative investigation is implemented with three conventional hysteresis models for MR elastomer base isolator: Bouc-Wen model, LuGre friction model and strain-stiffening model. The expressions of these models are given as follows:

Bouc-Wen model (Kwok *et al.* 2006, Charalampakis and Koumousis 2008)

$$F = k_0 x + c_0 \dot{x} + \alpha z + F_0 \tag{19}$$

$$\dot{z} = A\dot{x} - \beta|\dot{x}||z|^{n-1}z - \gamma\dot{x}|z|^n \tag{20}$$

where k_0, c_0, α, β, A, γ and n are parameters to be identified.

LuGre friction model (Yang *et al.* 2009)

$$F = k_0 x + c_0 \dot{x} + \frac{\beta}{\alpha} y + \frac{\varepsilon}{\alpha} y + F_0 \tag{21}$$

$$\frac{1}{\alpha}\dot{y} = \dot{x} - |\dot{x}|y \tag{22}$$

where k_0, c_0, α, β and ε are parameters to be identified.

Strain stiffening model (Li and Li 2019)

$$F = k_1 y + \alpha x^3 + F_0 \tag{23}$$

$$k_1 y = k_0(x - y) + c_0(\dot{x} - \dot{y}) \tag{24}$$

$$\alpha z^3 = c_1(\dot{x} - \dot{z}) \tag{25}$$

where k_0, c_0, k_1, c_1 and α are parameters to be identified.

All the models are identified based on the same experimental data from all sorts of loading conditions using proposed improved FOA. Besides, four-order Runge-Kutta method is adopted to iteratively solve the nonlinear differential equations in models. The RMS errors between actual measurements and model predictions, together with

parameter identification time, are employed as evaluation indices. Figs. 14(a) and (b) show the distributions of RMS errors and running time for four MR elastomer models, respectively. It can be seen that compared with LuGre friction model and strain stiffening model, Bouc-Wen model and proposed hybrid model have relatively smaller mean RMS and error ranges, which is between 0 and 15. Although the Bouc-Wen model has best identification accuracy, it needs the longest identification period among four models due to the multi-parameter and high nonlinearity in the model expression. Furthermore, Bouc-Wen, LuGre friction and strain stiffening models all have differential equations in model expressions, which will lead to iterative errors in the shear force prediction. This problem is able to further affect the prediction of control current signal, when these models are employed to design the semi-active controllers of MR elastomer isolator. The proposed hybrid model, with fewest model parameters and without any differential equations in model expression, outperforms other three models in terms of both computation efficiency as well as applicability for the controller design of MR elastomer isolator.

From the results in Figs. 12 and 13, it is clearly seen that the MR elastomer base isolator has the characteristic of field-dependence, which indicates that the parameters of proposed hybrid model developed for this smart device are

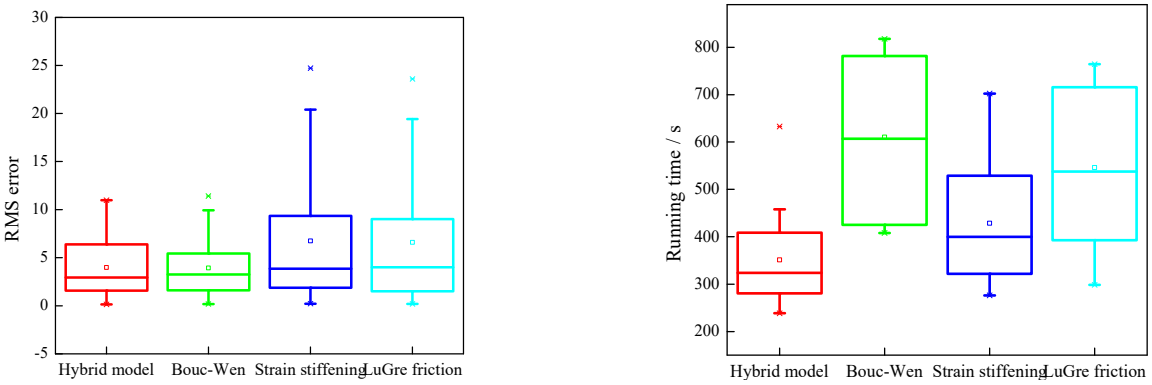

(a) RMS error (b) Identification time

Fig. 14 Performance evaluation of four MR elastomer models

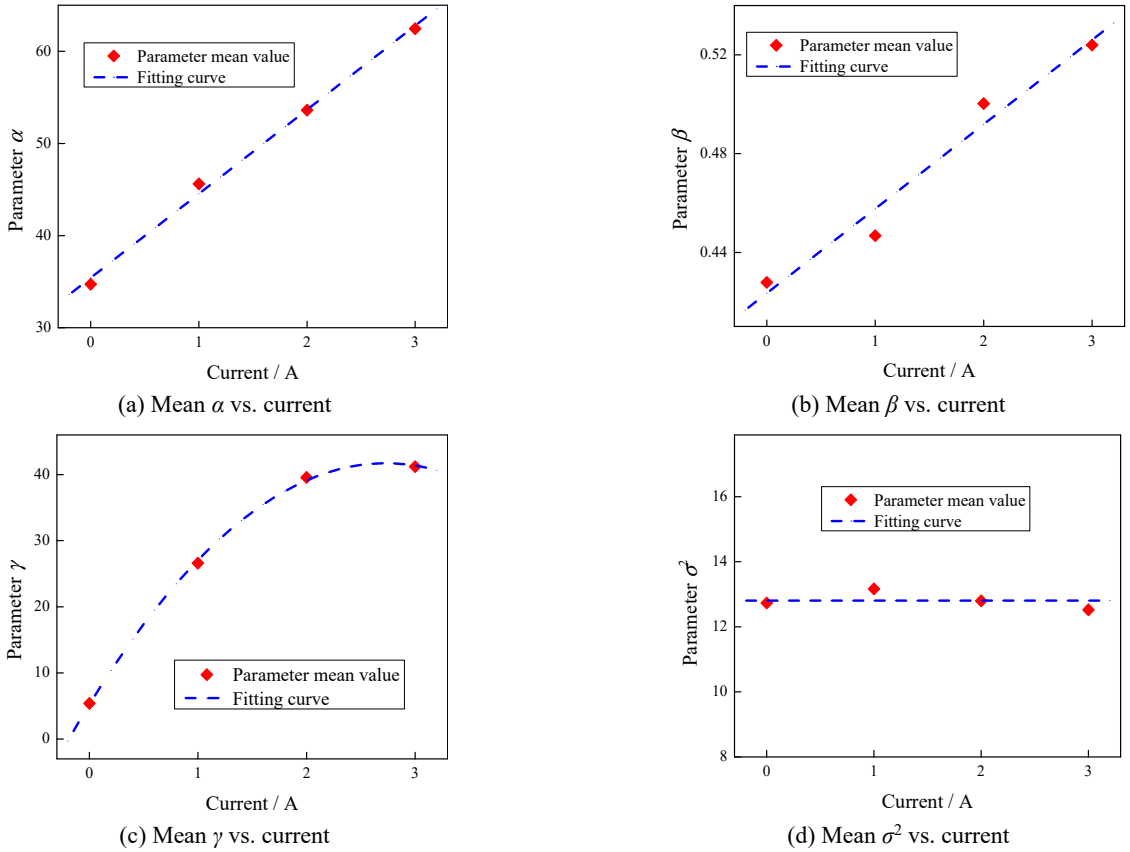

(a) Mean α vs. current (b) Mean β vs. current

(c) Mean γ vs. current (d) Mean σ^2 vs. current

Fig. 15 Relationships between mean parameter values and supply currents

affected by loading frequency, amplitude and applied current level. If we want to use the isolator for structural vibration mitigation, it is essential to investigate the relationships between model parameters and loading frequency/amplitude/applied current. However, in the practice, the external excitations are always unknown and could not be predicted in advance, which indicates that the loading frequency and amplitude are not controllable. The only controllable variable is the electric current applied to the MR elastomer base isolator. Accordingly, in this study, the parameter values estimated from different experimental conditions are divided into different groups in accordance with different current levels. Then, these values are averaged and the polynomial functions are employed to describe the relationships between mean values and applied current, shown in Fig. 15. Then, least square method is applied to calculate the coefficients in polynomial expressions, summarized as follows

$$\alpha = 9.121 \cdot I + 35.42 \tag{26}$$

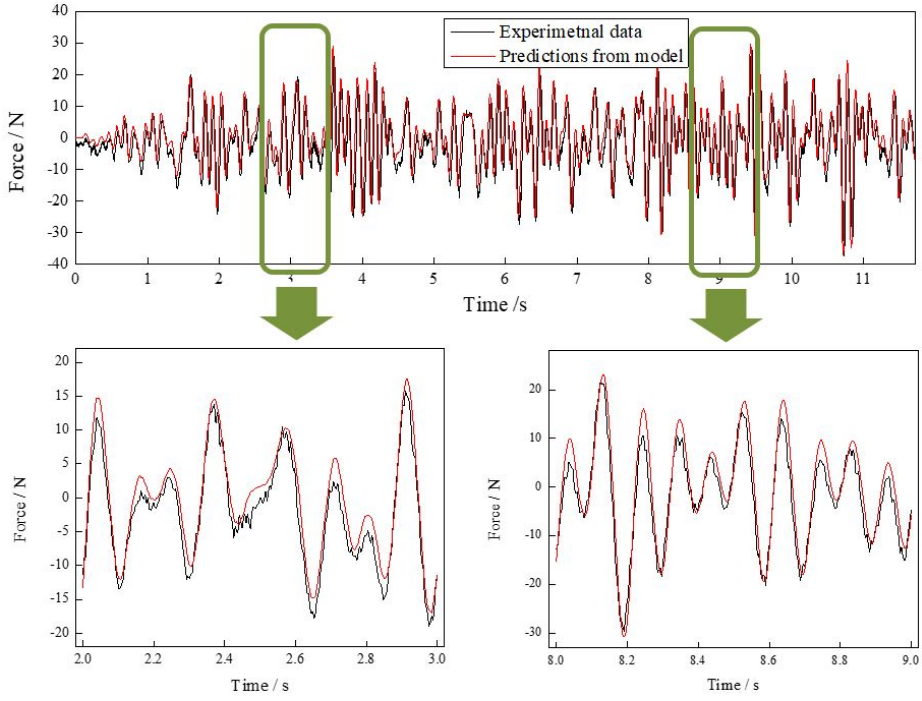

(a) 0A current

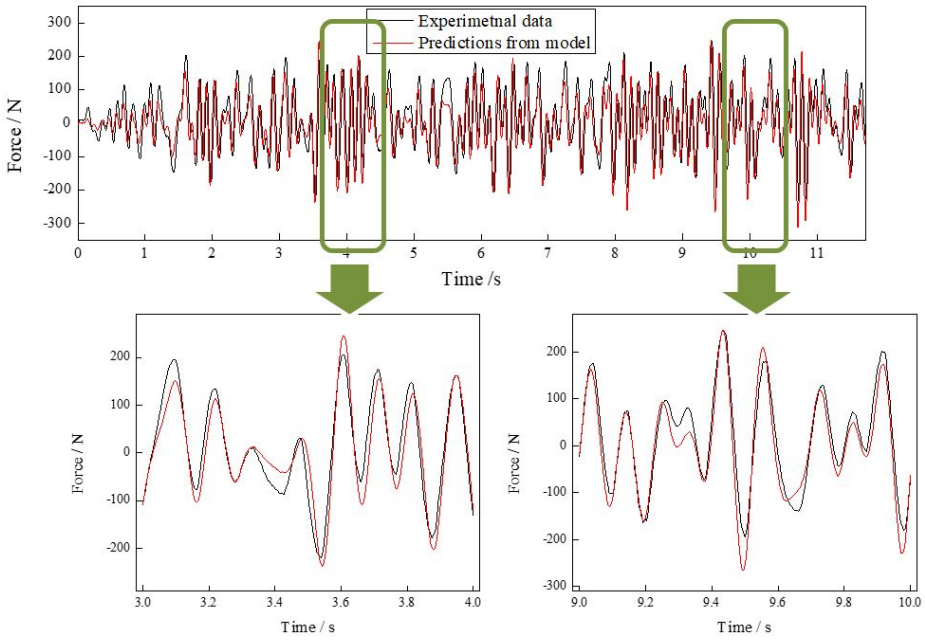

(b) 3A current

Fig. 16 Time-series response comparisons between measurements and model predictions when the random excitations are applied to the device

$$\beta = 0.0034 \cdot I + 0.4235 \quad (27)$$

$$\gamma = -4.892 \cdot I^2 + 26.72 \cdot I + 5.234 \quad (28)$$

$$\sigma^2 = 12.8059 \quad (29)$$

According to the results in Fig. 15, parameters α and β could be expressed based on first-order polynomial functions since they exhibit the linear relationships with supply current, which is more convenient and beneficial for the controller design. Parameter γ requires a second-order polynomial expression to indicate its relationship to applied current. Especially, it is noticed that the parameter σ^2 is around a constant corresponding to different current values. Based on these current-related parameters, the generalized model for MR elastomer base isolator is obtained with the following expression

$$F(x,I) = \begin{cases} F_1(x,I):\ \alpha(I) \cdot \dfrac{e^{2\beta(I)x} - 1}{2e^{\beta(I)x}} + \gamma(I)e^{-\frac{x^2}{2\sigma^2}} + F_0,\ \dot{x} \geq 0 \\ F_1(x,I):\ \alpha(I) \cdot \dfrac{e^{2\beta(I)x} - 1}{2e^{\beta(I)x}} - \gamma(I)e^{-\frac{x^2}{2\sigma^2}} + F_0,\ \dot{x} < 0 \end{cases} \quad (30)$$

In real situations, the loading frequencies of external excitations such as earthquakes or strong winds are always changed. Therefore, in this part the experimental data from the random excitations with variable frequencies between 1 Hz and 10 Hz are utilized to test the effectiveness of the proposed generalized current-dependent model. Fig. 16 presents the time-series comparisons between real measured forces and predicted responses when the isolator is passive (0 A) and is supplied with maximum current (3 A), respectively. It is clearly observed that the reconstructed responses satisfactorily fit with the experimental results in spite of several imperfections existing in parts of peak areas when the device is driven with 3 A current. Overall, this generalized model is able to well track the variation tendency of the device outputs with the variable external excitations, and can be considered as the ideal solution for establishing the controller to achieve real-timely adaptive vibration control of building structures using MR elastomer base isolators.

6. Conclusions

This paper adopts curve fitting method to design a new hysteretic model for demonstrating nonlinear behaviours of MR elastomer base isolator. This novel model, without any differential equation, just has four parameters to be identified, which is fewer than that of other classical MR elastomer models such as Bouc-Wen and LuGre friction models. To accurately estimate the model parameters, an improved fruit fly optimization algorithm is also proposed, in which traditional fixed step is replaced by a self-adaptive step, avoiding the local optimum in dealing with highly complicated optimization problems. Experimental data are used to establish and validate the capacities of the proposed model. The results indicate that compared with other MR elastomer models, the hybrid model is capable of sufficiently characterizing this novel device, and has optimal modelling accuracy as well as less calculation time.

Acknowledgments

The research described in this paper was funded by the Australian Research Council (Grant No. DP150102636) and the Natural Science Foundation of China (Grant No. 52002036). Besides, Dr. Yancheng Li of University of Technology Sydney is appreciated for the help in device design and test.

References

Aguirre, N., Ikhouane, F., Rodellar, J. and Christenson, R. (2012), "Parametric identification of the Dahl model for large scale MR dampers", *Struct. Control Hlth.*, **19**(3), 332-347. https://doi.org/10.1002/stc.434

Aziz, S.A.A., Mazlan, S.A., Ismail, N.I.N. and Choi, S.-B. (2018), "Implementation of functionalized multiwall carbon nanotubes on magnetorheological elastomer", *J. Mater. Sci.*, **53**(14), 10122-10134. https://doi.org/10.1007/s10853-018-2315-3

Bastola, A.K. and Li, L. (2018), "A new type of vibration isolator based on magnetorheological elastomer", *Mater. Des.*, **157**, 431-436. https://doi.org/10.1016/j.matdes.2018.08.009

Behrooz, M., Wang, X. and Gordaninejad, F. (2014), "Modeling of a new semi-active/passive magnetorheological elastomer isolator", *Smart Mater. Struct.*, **23**(4), 045013. https://doi.org/10.1088/0964-1726/23/4/045013

Besdo, D. and Ihlemann, J. (2003), "Properties of rubberlike materials under large deformations explained by self-organizing linkage patterns", *Int. J. Plast.*, **19**(7), 1001-1018. https://doi.org/10.1016/S0749-6419(02)00090-6

Charalampakis, A.E. and Koumousis, V.K. (2008), "Identification of Bouc-Wen hysteretic systems by a hybrid evolutionary algorithm", *J. Sound Vib.*, **314**(3-5), 571-585. https://doi.org/10.1016/j.jsv.2008.01.018

Fu, J., Lai, J., Yang, Z., Bai, J. and Yu, M. (2020), "Fuzzy-neural network control for a magnetorheological elastomer vibration isolation system", *Smart Mater. Struct.*, **29**(7), 074001. https://doi.org/10.1088/1361-665X/ab874d

Hwang, Y., Lee, C.W., Lee, J. and Jung, H.J. (2020), "Feasibility of a new hybrid base isolation system consisting of MR elastomer and roller bearing", *Smart Struct. Syst., Int. J.*, **25**(3), 323-335. https://doi.org/10.12989/sss.2020.25.3.323

Jiménez, R. and Álvarez-Icaza, L. (2005), "LuGre friction model for a magnetorheological damper", *Struct. Control Hlth.*, **12**(1), 91-116. https://doi.org/10.1002/stc.58

Kwok, N., Ha, Q., Nguyen, T., Li, J. and Samali, B. (2006), "A novel hysteretic model for magnetorheological fluid dampers and parameter identification using particle swarm optimization", *Sensor Actuat. A-Phys.*, **132**(2), 441-451. https://doi.org/10.1016/j.sna.2006.03.015

Leng, D., Sun, S., Xu, K. and Liu, G. (2020), "A physical model of

magnetorheological elastomer isolator and its dynamic analysis", *J. Intell. Mater. Syst. Struct.*, **31**(9), 1141-1156.

Li, Y. and Li, J. (2019), "Overview of the development of smart base isolation system featuring magnetorheological elastomer", *Smart Struct. Syst., Int. J.*, **24**(1), 37-52. https://doi.org/10.12989/sss.2019.24.1.037

Li, M.W., Geng, J., Hong, W.C. and Zhang, Y. (2018), "Hybridizing chaotic and quantum mechanisms and fruit fly optimization algorithm with least squares support vector regression model in electric load forecasting", *Energies*, **11**(9), 2226. https://doi.org/10.3390/en11092226

Lin, S.M. (2013), "Analysis of service satisfaction in web auction logistics service using a combination of Fruit fly optimization algorithm and general regression neural network", *Neural Comput. Appl.*, **22**(3-4), 783-791. https://doi.org/10.1007/s00521-011-0769-1

Mullins, L. and Tobin, N. (1957), "Theoretical model for the elastic behavior of filler-reinforced vulcanized rubbers", *Rubber Chem. Technol.*, **30**(2), 555-571. https://doi.org/10.5254/1.3542705

Neshat, M., Sepidnam, G., Sargolzaei, M. and Toosi, A.N. (2014), "Artificial fish swarm algorithm: a survey of the state-of-the-art, hybridization, combinatorial and indicative applications", *Artif. Intell. Rev.*, **42**(4), 965-997. https://doi.org/10.1007/s10462-012-9342-2

Nguyen, X.B., Komatsuzaki, T., Iwata, Y. and Asanuma, H. (2018), "Robust adaptive controller for semi-active control of uncertain structures using a magnetorheological elastomer-based isolator", *J. Sound Vib.*, **434**, 192-212. https://doi.org/10.1016/j.jsv.2018.07.047

Niu, J., Zhong, W., Liang, Y., Luo, N. and Qian, F. (2015), "Fruit fly optimization algorithm based on differential evolution and its application on gasification process operation optimization", *Knowl.-Based Syst.*, **88**, 253-263. https://doi.org/10.1016/j.knosys.2015.07.027

Pan, W.T. (2013), "Using modified fruit fly optimisation algorithm to perform the function test and case studies", *Connect. Sci.*, **25**(2-3), 151-160. https://doi.org/10.1080/09540091.2013.854735

Piatkowski, T. (2014), "Dahl and LuGre dynamic friction models - The analysis of selected properties", *Mech. Mach. Theory*, **73**, 91-100. https://doi.org/10.1016/j.mechmachtheory.2013.10.009

Sun, S.S., Yang, J., Li, W.H., Du, H., Alici, G., Yan, T.H. and Nakano, M. (2017), "Development of an isolator working with magnetorheological elastomers and fluids", *Mech. Syst. Signal Pr.*, **83**, 371-384. https://doi.org/10.1016/j.ymssp.2016.06.020

Tairidis, G., Foutsitzi, G., Koutsianitis, P. and Stavroulakis, G.E. (2016), "Fine tuning of a fuzzy controller for vibration suppression of smart plates using genetic algorithms", *Adv. Eng. Softw.*, **101**, 123-135. https://doi.org/10.1016/j.advengsoft.2016.01.019

Trivedi, R.R., Pawaskar, D.N. and Shimpi, R.P. (2016), "Optimization of static and dynamic travel range of electrostatically driven microbeams using particle swarm optimization", *Adv. Eng. Softw.*, **97**, 1-16. https://doi.org/10.1016/j.advengsoft.2016.01.005

Wen, Q., Wang, Y. and Gong, X. (2017), "The magnetic field dependent dynamic properties of magnetorheological elastomers based on hard magnetic particles", *Smart Mater. Struct.*, **26**(7), 075012. https://doi.org/10.1088/1361-665X/aa7396

Xin, F.-L., Bai, X.-X. and Qian, L.-J. (2017), "Principle, modeling, and control of a magnetorheological elastomer dynamic vibration absorber for powertrain mount systems of automobiles", *J. Intell. Mater. Syst. Struct.*, **28**(16), 2239-2254.

Yang, F., Sedaghati, R. and Esmailzadeh, E. (2009), "Development of LuGre friction model for large-scale magneto-rheological fluid dampers", *J. Intell. Mater. Syst. Struct.*, **20**(8), 923-937.

Yang, J., Du, H., Li, W., Li, Y., Li, J., Sun, S. and Deng, H.X. (2013), "Experimental study and modeling of a novel magnetorheological elastomer isolator", *Smart Mater. Struct.*, **22**(11), 117001. https://doi.org/10.1088/0964-1726/22/11/117001

Ying, Z.G., Ni, Y.Q. and Duan, Y.F. (2017), "Stochastic vibration suppression analysis of an optimal bounded controlled sandwich beam with MR visco-elastomer core", *Smart Struct. Syst., Int. J.*, **19**(1), 21-31. https://doi.org/10.12989/sss.2017.19.1.021

Yousefi, A.M., Samali, B. and Hajirasouliha, I. (2020), "Experimental and numerical investigations of cold-formed austenitic stainless steel unlipped channels under bearing loads", *Thin Wall. Struct.*, **152**, 106768. https://doi.org/10.1016/j.tws.2020.106768

Zhang, X. and Li, W. (2009), "Adaptive tuned dynamic vibration absorbers working with MR elastomers", *Smart Struct. Syst., Int. J.*, **5**(5), 517-529. https://doi.org/10.12989/sss.2009.5.5.517

Zhang, X., Lu, X., Jia, S. and Li, X. (2018), "A novel phase angle-encoded fruit fly optimization algorithm with mutation adaptation mechanism applied to UAV path planning", *Appl. Soft. Comput.*, **70**, 371-388. https://doi.org/10.1016/j.asoc.2018.05.030

Zhou, X., Sun, J., Li, H., Lu, M. and Zeng, F. (2020), "PMSM open-phase fault-tolerant control strategy based on four-leg inverter", *IEEE T. Power Electr.*, **35**(3), 2799-2808. https://doi.org/10.1109/TPEL.2019.2925823

Zhu, W. and Rui, X.T. (2014), "Semiactive vibration control using a magnetorheological damper and a magnetorheological elastomer based on the bouc-wen model", *Shock Vib.*, **2014**, 405412. https://doi.org/10.1155/2014/405421

HJ